Calculation of H(1*s*) angular distributions for H^+ impinging on Al(111) at grazing incidence

F. A. Gutierrez[1] and H. Jouin[2,*]

[1]*Departamento de Física, Universidad de Concepción Casilla 160-C, Concepción, Chile*

[2]*CELIA (UMR 5107 Université Bordeaux 1-CNRS-CEA), Université Bordeaux 1, 351 Cours de la Libération, F-33405 Talence Cedex, France*

(Received 12 May 2010; published 29 June 2010)

We have computed angular distributions of scattered ground-state hydrogen atoms after interaction of 49-, 25-, 6.25-, and 1-keV proton beams with an Al(111) surface under a grazing angle of incidence of 0.56°. Capture and loss for resonant and Auger processes are taken into account, as well as the surface-plasmon-assisted electron-capture mechanism. Consideration of all these processes makes it possible to obtain a good agreement with the available experimental result at 25 keV ($v = 1$ a.u.). For the other impact energies considered, our predictive results have to be compared to measurements; such comparisons could make it possible to discriminate between the various theoretical results available in the literature for the resonant process which are used in the present dynamical calculations.

DOI: 10.1103/PhysRevA.81.062901 PACS number(s): 79.20.Rf, 73.20.Mf, 79.20.Fv

I. INTRODUCTION

The study of electron exchange between singly charged ions or neutral atoms and metal surfaces at grazing incidence has been notably increased during the past two decades (see, for instance, [1] and references therein).

In a recent work [2], by means of the ETISC1D code for dynamical calculations [3], we computed outgoing H(1*s*) fractions in the velocity range $0.1 \leqslant v \leqslant 2.0$ a.u. for protons impinging on Al(111) with a grazing angle of incidence of 0.5°. The role of capture and loss for both resonant and Auger processes was investigated together with the relevance of the surface-plasmon-assisted electron-capture channel, which is closed within the fixed ion approximation [2]. Consideration of all these mechanisms together yields a good agreement between a set of theoretical H(1*s*) fractions and the experimental data of Winter [1]. Major ingredients of these calculations were: (a) the accurate dynamical image potential of Garcia de Abajo and Echenique [4] for ions traveling parallel to an Al surface, (b) velocity-dependent resonant and Auger transition rates which we obtained [2] from the corresponding static rates reported in the literature ([5–7] for the resonant mechanism and [8] for the Auger process) through the approximate "kinematic factors" approach proposed by Mišković and Janev [9], and (c) velocity-dependent pure surface-plasmon (PSP) rates which contribute in a non-negligible way to the ion neutralization [2,10].

Besides the aforementioned good agreement between the theoretical and the experimental neutral fractions, we found that the resonant processes play the major role for $v \lesssim 1.5$ a.u., while at higher velocities Auger capture and loss mechanisms mainly explain the experimental findings. These ranges of relevance for the resonant and Auger modes are in agreement with earlier qualitative conclusions of Zimny *et al.* [11] for the same system, although we showed that their total neutral fractions are somewhat inacurate due to the approximate method used by them to solve their rate-equations system. It was also found that the effect of the collective surface-plasmon mode is noticeable for $0.5 \leqslant v \leqslant 1.2$ a.u., with a significant contribution to the neutral fraction around the Fermi velocity ($v_F \simeq 0.9$ a.u.).

An interesting finding was that although for the resonant width (i.e., static resonant capture rate) we considered three different reports [5–7] which present large discrepancies [either quantitatively for the magnitude of the static capture rates or qualitatively for the behavior of the H(1*s*) energy near the metal], the corresponding outgoing H(1*s*) fractions show rather weak differences at low and high velocities, while in the intermediate velocity range (around $v = 1$ a.u.) there are no variations at all. These weak differences between the three computed outgoing H(1*s*) fractions can be traced back to the sensitivity of both resonant and Auger kinematic factors to the atomic energy of the perturbed (by the nearby metal surface) hydrogen atom which can be produced and ionized several times along its trajectory. Therefore, it seems that the final neutral fractions are more strongly determined by the simultaneous interplay between capture and loss and also by the time-dependent population of the interacting states than by the magnitude of the static capture rates of the participating modes.

On the other hand, around two decades ago a few experimentalists started to report direct measurements of another physical quantity (besides neutral fractions) which, for a given incident velocity of the projectile, yields more detailed information about the dynamics of the ion (or atom)-metal grazing collision with electron exchange. Such quantity is the angular distribution (AD) of the scattered species which have been reported experimentally by Winter and collaborators for various systems [1].

Due to the large amount of information provided by the AD as compared to the neutral fraction (NF), which for a particular value of the velocity is just one number (corresponding to the integral of the AD), it is expected to be more sensitive than the NFs to the ingredients considered in its evaluation. Indeed, a complete agreement between the theoretical and the experimental ADs requires not only a good match of their width and shape but also a good match of the height and the angular location of their distribution's peak. As the evaluation of both physical quantities requires the same set of ingredients, the information provided by the AD and the NF should be

*jouin@celia.u-bordeaux1.fr

taken together in order to get a complete picture of the role and the relevance of each ingredient in the charge-transfer processes. More than that, in our approach to the study of ion- or atom-metal grazing collisions with electron exchange, both quantities are consistently and simultaneously obtained within the ETISC1D code [3].

Furthermore, it is not hard to visualize the fact that a correct AD leads necessarily to the correct NF while the inverse is not true because the evaluation of a NF includes the counting of all the final neutral atoms independent of their angular position. As a consequence, two different ADs (with respect to shape, width, height, or angular position) can lead to the same NF. Therefore, although at a given incident velocity there is a connection between the AD and the NF (since the NF corresponds to the integral of the AD), it is obvious that the former cannot be uniquely defined by the value of the latter.

Thus, in the present work we have first calculated ADs for 25-keV H^+ projectiles impinging on an Al(111) surface under an angle of incidence of 0.56° in order to compare them with the experimental data reported by Winter and Sommer [12]. We are interested to find out:

(a) if the good agreement obtained between theory and experiment for the NF of the H^+-Al(111) interaction at 25 keV [2] is still present for the corresponding AD;

(b) how much and also in what way the AD for this interaction gets affected by the various results used for the resonant mode;

(c) the dependence of the AD on the ion-surface image potential (if there were no dependence or if its effect appears only as a shift of the whole distribution, then the corresponding NF would be independent of the form of the image potential, an aspect which was not considered in [2]);

(d) the relevance of the individual contributions, from each neutralization and ionization channel, when compared with the experimental AD.

Furthermore, we also want to study if for smaller or larger energies the rather weak differences exhibited by the NFs, due to the different behavior of the resonant modes, show up also in the AD, although in this case we shall not be able to make comparisons with experiments since, for this system, we have not found in the literature experimental ADs for energies other than 25 keV.

In Sec. II we briefly analyze both the theory and the simulations behind the present evaluations of the AD together with its ingredients (ion-surface interaction potentials and velocity dependence of the capture and loss rates for each channel). The corresponding results for various velocities of H^+ projectiles impinging on an Al(111) surface under an angle of incidence of 0.56°, followed by the relevant discussions, are included in Sec. III. First we consider the case $v = 1.0$ a.u. for which we can make comparisons with the experimental AD of Winter and Sommer [12]. Afterward we consider the cases $v = 1.4$ and 0.5 a.u. for which the corresponding NFs [2] show clear differences among the different resonant rates, a situation which does not occur at 25 keV ($v = 1.0$ a.u.). Therefore, for these cases we expect to find differences between the AD connected with the different resonant rates. Finally, we consider the case $v = 0.2$ a.u. in the range of velocities ($0.0 \leqslant v \leqslant 0.3$ a.u.) for which the NFs are the same [2] for the different resonant rates, yielding total neutralization of the beam. This case appears to be a good example of a situation where very different ADs yield the same NF. Final conclusions and future directions are given in Sec. IV. Atomic units are used throughout this article unless otherwise stated.

II. ANGULAR DISTRIBUTIONS: THEORY AND INGREDIENTS

Dynamical calculations have been performed by means of the semiclassical ETISC1D code [3] constructed for grazing-incidence particle-surface collisions. The particle's parallel velocity ($v_\parallel$) is kept constant while the perpendicular motion of the ionic (or atomic) species is obtained by integration of Hamilton-Jacobi equations in which the scattering potential is changed when the charge state of the species varies due to an electron charge-transfer process. These latters are taken into account through their respective transition rates complemented by a Monte-Carlo-type procedure that make it possible to simulate the possibility of an electronic transition during a time step corresponding to the integration of Hamilton-Jacobi equations. In that way, one obtains the position, the momentum, and the internal state of each particle of the beam at every time. In the simulations presented in what follows, we have used beams containing typically 9×10^5 particles in order to have good statistics.

Simulations are performed inside a simulation box whose lower limit corresponds to the position of the first atomic layer while the upper bound ($z_{\max}$: typically some tens of a.u.) is chosen so that, at $z_{\max}$, all the transition rates relevant for the case studied are negligible with respect to their maxima close to the surface. One can verify that $z_{\max}$ is large enough by checking that no electronic transition occurs during the first integration time steps. Moreover, in the incoming pathway, when a particle penetrates into the simulation box at $z_{\max}$, its momentum has to be defined according to its initial charge state. Indeed, initially charged particles which feel asymptotically the long-range attractive image potential are accelerated before entering in the simulation box. Hence, their momentum at $z_{\max}$ must be defined as their initial perpendicular momentum increased by the momentum that they gain during their travel between ∞ and $z_{\max}$. Conversely, impinging neutrals feel a repulsive short-range potential which vanishes asymptotically. In that way, their momentum at $z_{\max}$ is simply their initial perpendicular momentum. Obviously, we always check that the results (charge fractions and ADs) do not depend on the bounds of the simulation box.

In the outgoing path, when a neutral particle leave the simulation box, its final perpendicular velocity ($v_\perp^f$) make it possible to calculate the corresponding outgoing angle φ (with respect to the surface plane) through the equation $\tan\varphi = v_\perp^f / v_\parallel$. By counting each particle in a given charge state according to its outgoing angle, we compute the primary AD of scattered particles in a defined final charge state. The widths of these distributions are completely determined by the charge-exchange processes (and the related changes of scattering potential) experienced by the particles during their travel in the vicinity of the surface.

However, these primary ADs account for neither the corrugation effects on the particle's trajectories nor the experimental angular resolution. Both of these effects produce a broadening

of the primary AD. In the typical Winter's measurements the experimental angular resolution is around $\delta\varphi = 0.1^\circ$ [13] and it is a simple matter to take into account this effect in the theoretical result by performing a convolution of the primary AD by a Gaussian shape of width $\delta\varphi$. Concerning rugosity effects, a three-dimensional simulation (or at least a two-dimensional one) should be necessary to properly account for these phenomena, but obviously such simulations would be much more time consuming than the present monodimensional ones. In order to overcome this difficulty and to account, at least in an approximate way, for corrugation, in our procedure the primary AD is convoluted by means of a Gaussian function of full width at half maximum (FWHM) $\Delta\phi$ which accounts for both effects (experimental resolution and rugosity). In what follows, we report calculations of H(1s) ADs for H^+ impinging on Al(111) with an angle of incidence $\Phi_{in} = 0.56^\circ$ and for the four velocities $v = 0.2$, 0.5, 1.0, and 1.4 a.u. In the case $v = 1$ a.u., in which an experimental result is available [12], we have used for $\Delta\phi$ the FWHM of the experimental H(1s) AD: $\Delta\phi(v = 1) = 0.65^\circ$. It is known that the enlargement due to corrugation increases with velocity for a given angle of incidence. In order to account for this effect in the forthcoming AD, we have taken for the three other velocities: $\Delta\phi(v = 0.2) = 0.4^\circ$, $\Delta\phi(v = 0.5) = 0.5^\circ$, and $\Delta\phi(v = 1.4) = 0.8^\circ$. Finally, the area of the resulting convoluted AD is normalized to the outgoing charge fraction of the corresponding charge state which is also obtained at the end of the simulation when all particles have left the simulation box.

In our comparisons to measurements, the experimental ADs are normalized in the same way to the experimental outgoing charge fraction of the corresponding particles. This procedure makes it possible to perform a fair and complete comparison between theory and experiments for ADs.

In the case $v = 1$ (25 keV), the experimental NF is around 50% [1] for an angle of incidence of 0.5°. In the present case, the angle of incidence is 0.56° and as a consequence, the corresponding initial perpendicular velocity is slightly higher than in the 0.5° case. For this reason, the experimental H(1s) AD used in what follows has been normalized to 49% since it is known that the importance of charge-exchange processes decreases with increasing initial perpendicular velocity.

Two fundamentals physical inputs of these simulations are the scattering potential corresponding to each relevant charge state (+1 and 0 in the present case) and the transition rates related to every charge-exchange process involved.

A. The projectile-surface potentials

The purely repulsive potential felt by hydrogen atoms, at a distance s from the image plane, $U_0(s)$, is obtained by averaging over the first atomic plane individual interatomic potentials represented by a Ziegler-Biersack-Littmark (ZBL) screening function [14]. The potential $U_+(s, v_\parallel)$ experienced by protons is described as the sum of the planar potential $U_0(s)$ plus the attractive dynamical image potential $U_I(s, v_\parallel)$. Here we have considered two different descriptions of this potential, the most sophisticated one being that obtained by García de Abajo and Echenique (GAE) [4] within the specular-reflection model in the random phase approximation. Since the evaluation of this potential within a dynamical code such as the ETISC1D makes it very time consuming, we have fitted it for a trajectory parallel to an Al surface as

$$U_I^{\mathrm{GAE}}(s, v_\parallel) = \begin{cases} -\frac{1}{4s}(1 - e^{-\alpha s}) + \frac{b}{s^2}(1 - e^{-\beta s^2}) & \text{for } s > 0 \quad (1a) \\ -U_S\left[1 + A\, e^{\gamma s - \delta s^2}\right]^{-1} & \text{for } -d_{\mathrm{im}} \leqslant s \leqslant 0, \quad (1b) \end{cases}$$

where the parameters α, b, and β corresponding to the external part ($s > 0$) are first determined. For the internal part ($s \leqslant 0$), only U_S and δ correspond to free parameters since A and γ are obtained by matching at $s = 0$ the expressions of Eqs. (1a) and (1b) as well as their first derivatives. The relevant set of parameters for H^+ traveling parallel to an Al surface in the range $0.0 \leqslant v_\parallel \leqslant 2.8$ has been reported in Ref. [2]. For velocities other than those included in Table 1 of Ref. [2], the parameters can be determined by interpolation. In Eq. (1b), d_{im} is the distance between the first atomic layer and the image plane ($d_{\mathrm{im}} = 3.295$ a.u. for Al(111) [15]).

These fits make it possible to reproduce very closely [2] the numerical GAE dynamical image potential yielding a total potential $U_+^{\mathrm{GAE}}(s, v_\parallel)$ whose variations are rather weak for $v_\parallel \leqslant 1.5$, with their most significant spatial variation being the decrease of the potential's slope in the image plane region ($s \approx 0$) for increasing velocities as can be seen in Fig. 1(a), where U_+^{GAE} is plotted for the four velocities considered in this work. To make more explicit the variation of U_+^{GAE} near the surface, which relates directly to the strength of the force in the z direction and as a consequence on the change of momentum of the projectile [3], we include in Fig. 1(b) the derivative of U_+^{GAE} as a function of the ion-surface distance for the same velocities considered for U_+^{GAE} in Fig. 1(a).

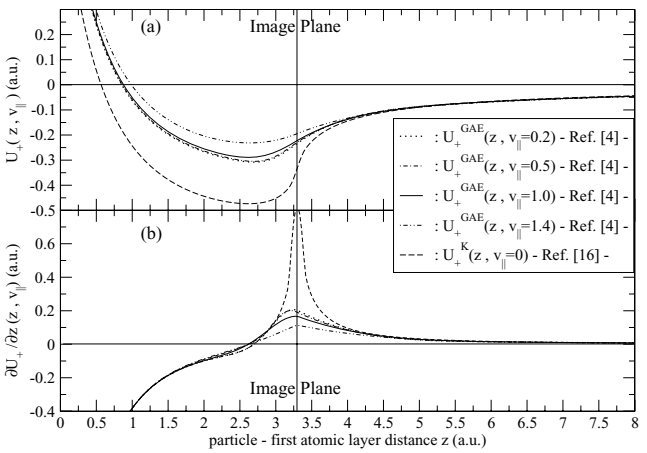

FIG. 1. (a) Potential $U_+(z, v_\parallel)$ [felt by protons, $U_+(z, v_\parallel) = U_0(z) + U_I(z, v_\parallel)$] as a function of the H^+-first atomic layer distance (z). (b) $\partial U_+(z, v_\parallel)/\partial z$ as a function of z. In all cases the planar repulsive potential $U_0(z)$ is obtained from the ZBL screening function. Dotted line, dynamical $U_+^{\mathrm{GAE}}(z, v_\parallel = 0.2)$ potential obtained by means of the dynamical image potential $U_I^{\mathrm{GAE}}(z, v_\parallel = 0.2)$ of Garcia de Abajo and Echenique [4]; dot-dashed line, $U_+^{\mathrm{GAE}}(z, v_\parallel = 0.5)$; solid line, $U_+^{\mathrm{GAE}}(z, v_\parallel = 1.0)$; dot-dot-dashed line, $U_+^{\mathrm{GAE}}(z, v_\parallel = 1.4)$; dashed line, static $U_+^{K}(z, v_\parallel = 0)$ potential obtained by using the static Thomas-Fermi image potential $U_I^{K}(z, v_\parallel = 0)$ proposed by Kato *et al.* [16].

Note that for $v_\parallel < 0.5$ the curves for both U_+^{GAE} and its derivative go very close to each other in the whole range of distances. Furthermore, for purposes of comparison, we also consider in this work the alternative static ($v_\parallel = 0$) description of the image potential $U_I^K(s)$ proposed by Kato *et al.* in Ref. [16], which is based on the Thomas-Fermi approximation and which was already considered in Ref. [17] for studying the He^+-Al system. The corresponding potential $U_+^{\mathrm{TF}}(s) = U_0(s) + U_I^{\mathrm{TF}}(s)$ and its derivative are also included in Figs. 1(a) and 1(b). It is clear that for all velocities the potential U_+^{TF} should have a much larger effect on the ions than U_+^{GAE} close to the image plane. We want to analyze if this difference between both potentials shows up with a noticeable effect on the AD.

B. Velocity-dependent neutralization modes

Since for the H-Al system the atomic ground state at large atom-surface separations lies slightly (≈2.2 eV) above the bottom of the conduction band and is shifted upward at finite distances due to image effects, resonant electron capture (RC) is an efficient mechanism for populating this atomic state complemented by the Auger electron capture (AC) and the PSP process, which becomes open for Al only at finite velocities [2,10]. Working in the rest frame of the moving projectile, the Fermi sphere appears Galilean shifted in momentum space, modifying the RC and AC transition rates with respect to the static case and allowing to the captured electron to return back to the solid via resonant electron loss (RL) or Auger electron loss (AL). As in earlier works [2,10] and based on experimental grounds, we do not consider here the small contributions of excited states. We also note that as in Ref. [2] the surface-plasmon-assisted electron-loss process, which is possible in principle [18], has been neglected in the present work as (at least) a second-order effect. Indeed, not only is the energetic constraint for this collective mechanism much more stringent than that for Auger loss, it also needs a significant population of already-excited surface-plasmons on the surface as the protons approach it to become efficient as an ionizing process.

1. Static rates for the resonant and Auger modes

Several nonperturbative calculations have been performed to obtain the width [i.e., the static resonant capture transition rate $\Gamma_{\mathrm{RC}}^g(s, v_\parallel = 0)$] and the energy $E_g(s)$ of the hydrogen ground state in front of an Al surface. Presently, the most relevant results seem to be those of Nordlander and Tully [5], Borisov *et al.* [6] (whose results are very close to those of Martín and Politis [19]), and Deutscher *et al.* [7]. Unfortunately, these results show important discrepancies mainly due to the extreme sensitivity of the hydrogen ground-state width and energy to the structure of the electron-surface potentials in the near-surface region. Indeed, in the whole range of relevant distances, the width obtained by Deutscher *et al.* [7] is around a factor of 2 greater than the one computed by Nordlander and Tully [5], while this latter is four times greater than the results reported by Borisov *et al.* [6]. Furthermore, although at large and intermediate distances the energy curves obtained in these three works follow the classical $-1/4s$ image behavior, for $s \lesssim 4$ they split apart with the energy in Ref. [6] keeping the $-1/4s$ dependence contrary to the curve of Ref. [7], which reaches a maximum around $s = 3.5$, decreasing afterward down to almost the free atom value at $s = 1$ while the energy reported in [5] gets intermediate between the two other ones. Another relevant report, which gives ground-state energy curves and static transition rates falling between those of Refs. [5] and [7] is that of Kurpick *et al.* [20]. Therefore, the effects contained in their results will be covered by the range of values included in Refs. [5–7], so we do not analyze them explicitly. We obtain ADs for these three static descriptions of the resonant mode after inclusion of velocity effects on the transition rates, as indicated in the following section.

On the other hand, to our knowledge, calculations of static two-electron Auger capture rate $\Gamma_{\mathrm{AC}}^g(s, v_\parallel = 0)$ toward the ground state, which are very involved, have been performed only by Hentschke *et al.* [8] by means of a perturbative approach, so we consider them in the present calculations.

It must be also noted that both the static rates (resonant and Auger) and static energy levels are only available (Refs. [5–7,19,20]) for distances above the image plane. For this reason, we assume vanishing resonant and Auger rates behind the image plane in the following calculations. The good agreement between theory and experiments for NFs within the whole range of relevant energies [2] and also for ADs at 25 keV, as is shown in what follows, seems to indicate that this is a reasonably good approximation whose theoretical explanation is beyond the scope of the present work.

2. Velocity-dependent rates for all modes

To obtain velocity-dependent transition rates from the static ones for both resonant and Auger transitions, we use the approximate method of Mišković and Janev [9]. The assumption that matrix elements are isotropic in **k** space makes it possible to factorize the ion velocity ($v_\parallel$) dependence of the rates into what are called *kinematic factors* [9,11]. For the RC and RL processes this assumption leads to the *resonant kinematic factors* $K^{\pm}\big(E_f(s), v_\parallel\big)$, so that

$$\Gamma_{\mathrm{RC,\,RL}}(s, v_\parallel) = K^{\pm}\big(E_f(s), v_\parallel\big)\, \Gamma_{\mathrm{RC}}(s, v_\parallel = 0), \tag{2}$$

with K^+ for RC and K^- for RL. These factors which depend implicitly upon s through the particle-image plane distance dependence of the final atomic state energy $E_f(s)$ [i.e., $E_g(s)$ in the present case], read as follows:

$$K^+(E, v_\parallel) = \langle f \rangle \left(\varepsilon = \frac{E}{E_F}, r_\parallel = \frac{v_\parallel}{v_F} \right) \tag{3a}$$

$$K^-(E, v_\parallel) = 1 - K^+(E, v_\parallel), \tag{3b}$$

where v_F and E_F are the Fermi velocity and Fermi energy, respectively and $\langle f \rangle(\varepsilon, q)$ is the angle-averaged Fermi-Dirac distribution for a jellium at zero temperature, which has been already reported in the literature [9,11].

On the other hand, for the AC and AL processes, the assumption of k-isotropic Auger matrix elements makes it possible to factorize the ion velocity ($v_\parallel$) dependence of the rates into *Auger kinematic factors* $Q^{\pm}\big(E_f(s), v_\parallel\big)$, so that

$$\Gamma_{\mathrm{AC,\,AL}}(s, v_\parallel) = Q^{\pm}\big(E_f(s), v_\parallel\big)\, \Gamma_{\mathrm{AC}}(s, v_\parallel = 0), \tag{4}$$

with Q^+ for AC and Q^- for AL. As in the resonant case, these factors depend upon s through the particle-image plane distance dependence of the final atomic-state energy $E_f(s)$ and they read

$$Q^{\pm}(s,v_{\parallel}) = \int_0^{+\infty} dE\, n(E)\, K^{\mp}(E,v_{\parallel}) \times T^{\pm}\left\{\frac{1}{2}[E+E_f(s)],v_{\parallel}\right\}, \quad (5)$$

where the integration variable E is referred to the bottom of the conduction band, $K^{\pm}(E,v_{\parallel})$ are the resonant kinematic factors already given in Eqs. (3), and $n(E)$ is the metal density of states, which is identified here with the unperturbed bulk density of levels per spin: $n(E) = \frac{3}{4}E_F^{-\frac{3}{2}}\sqrt{E}\,\Theta(E)$, with $\Theta(E)$ the unit step function. The $T^{\pm}(x,v_{\parallel})$ functions are obtained through

$$T^{\pm}(x,v_{\parallel}) = \frac{\int_{-\infty}^{+\infty} dy\, n(x+y)n(x-y)K^{\pm}(x+y,v_{\parallel})K^{\pm}(x-y,v_{\parallel})}{\int_{-\infty}^{+\infty} dy\, n(x+y)n(x-y)}, \quad (6)$$

where the numerators are the so-called "Auger transforms" [9], while the denominator is the self-convolution of the bulk density of states. Even with the simple analytical formula for both the density of states and the averaged Fermi-Dirac distribution, calculations of both $T^{\pm}$ functions and $Q^{\pm}$ factors are much more involved than those needed for $K^{\pm}$ and lead to very lengthy semianalytical expressions. Evaluation of $K^+(E_f(s),v_{\parallel})$ and $Q^+(E_f(s),v_{\parallel})$ for different velocities as functions of s together with a detailed analysis of their behavior is given elsewhere [2], where it has been seen that our calculations of $Q^{\pm}$ and $K^{\pm}$ agree with those reported in [9,11].

One has to note that various of the parameters of the active electron-surface potential [21] considered in the calculations of the ground-state energy $E_g(s)$ of the hydrogen atom near the metal surface [6,7,19] are known ([21] and references therein) to have a weak dependence on the particle's velocity, which pushes the image plane a little bit closer to the jellium edge. Therefore, the energy $E_g(s)$ of the final atomic state may have a small velocity dependence, which we expect to be negligible for our present purposes.

For $v_{\parallel} = 1.0$ (25 keV), capture and loss transition rates for both the resonant mode and the Auger mode are given in Fig. 2 for the three static results (width and energy) reported in Refs. [5–7] (Ref. [5], Calc. I; Ref. [6], Calc. II; and Ref. [7], Calc. III). We note that, for consistency, to obtain the velocity-dependent Auger rates of Calculations I–III through the kinematic factors $Q^{\pm}$, we have used the static ground-state energy related to the corresponding resonant cases of Refs. [5–7], respectively. For purposes of completeness, we also include for the same velocity the PSP rate for neutralization mode evaluated elsewhere [2,10]. The three resonant rates for both capture and loss channels show clear differences between them as the corresponding widths in the static case [2]. Furthermore, for these cases the capture and the loss channel curves go very close to each other with the latter rates slightly above the former ones, a situation which we have found is always present for $v_{\parallel} > v_F \simeq 0.9$. On the other hand, when $v_{\parallel} = v_F$ the capture and loss channel curves go on top of each other, while for $v_{\parallel} < v_F$ the capture rate overcomes the loss rate. For the Auger capture channel the curves in Calculations I and III do not differ very much, while curve II gives noticeably smaller rates due to the behavior of the H(1s) energy level of Ref. [6] at short distances. On the other hand, the Auger loss curves are very similar in the three cases. As in the resonant case, we have found that for the Auger mode the ratio between loss and capture is clearly larger than 1 for $v_{\parallel} > v_F$ equal to 1 when $v_{\parallel} = v_F$ and smaller than 1 when $v_{\parallel} < v_F$.

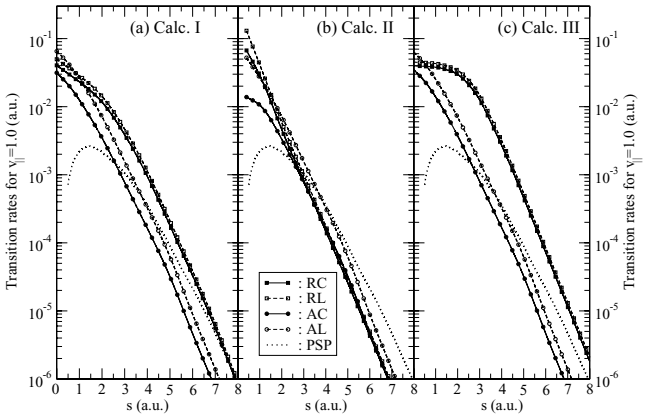

FIG. 2. $v_{\parallel} = 1$ a.u. (25-keV) transition rates for RC (solid squares), RL (open squares), AC (solid circles), AL (open circles), and PSP (dotted line) processes as a function of the particle-image plane distance (s). (a) Calculation I, based on static results of Refs. [5] and [8]; (b) Calculation II, based on static results of Refs. [6] and [8]; (c) Calculation III, based on static results of Refs. [7] and [8] (see text).

The relative behavior of the rates for the three channels depends on the particular case (I, II, or III) under consideration: In cases I and III, and for almost all of the relevant range of ion-surface distances, the resonant (capture and loss) rates are larger than the Auger (capture and loss) rates and also larger than the PSP capture rates. Only in the very small region $s \lesssim 0.5$ does the Auger loss slightly overcome the resonant rates. In case II the situation appears more complicated with the resonant (capture and loss) rates slightly above the Auger (capture and loss) rates and well above the collective capture rate only at short ion-surface distances while at intermediate and large distances it is the collective capture rate that goes above the resonant and Auger rates which, for this range of distances, do not differ too much from each other. Moreover, in the three cases (I, II, and III), at intermediate and large ion-surface distances, the PSP capture rate is larger than the capture and loss Auger channels. A similar result was found for the capture channel of the He^+-Al system at low velocities [22], where a reasonable qualitative explanation for this situation was given. We note that only the collective capture channel shows a maximum of its probability rate, which indicates that this process is more likely to occur at distances not close to the surface.

It is also relevant to note that for a two-species system the change in the number of particles of species 1 is proportional not only to the transition probability for that species but also to the number of particles of species 2. Therefore, the increment of one of the species (H^0 or H^+ in the present case) during

the projectile-surface interaction occurs at the expense of the other. In particular for an incident proton (H^+) beam, the initial number of hydrogen atoms (H^0) in such a beam is zero, so that even when the loss transition probability overcomes the capture transition probability there will be a much larger number of electrons captured by the beam than loss of them.

III. RESULTS AND DISCUSSION

A. The case of 25-keV incident energy

In Fig. 3 we present normalized ADs as functions of the scattering angle of H(1*s*) atoms after grazing collisions (0.56°) of 25-keV H^+ ions with an Al(111) surface. These results include the simultaneous contribution of the capture and loss channels for both resonant (R) and Auger (A) modes plus the capture channel for the plasmon (P) mode. It contains three curves for theoretical ADs which correspond to the aforementioned results of Nordlander and Tully [5] (I-RAP), Borisov *et al.* [6] (II-RAP) and Deutscher *et al.* [7] (III-RAP), respectively, for the static resonant transitions rates. Also included in Fig. 3 are the normalized experimental ADs of Winter and Sommer [12] for incident protons.

From Fig. 3 we see that there is a pretty good overall agreement between the theoretical curves and the experimental data which is consistent with the close values of their corresponding NFs [2] (I-RAP, 48.8%; II-RAP, 48.6%; and III-RAP, 48.5%). A small difference between all the theoretical curves with the experimental data occurs for a small angular range (2.0°–2.3°) at the right tail of the distributions where their values are more than one order of magnitude smaller than at their peaks. These weak differences can be traced back to the approximate method used in our simulations to account

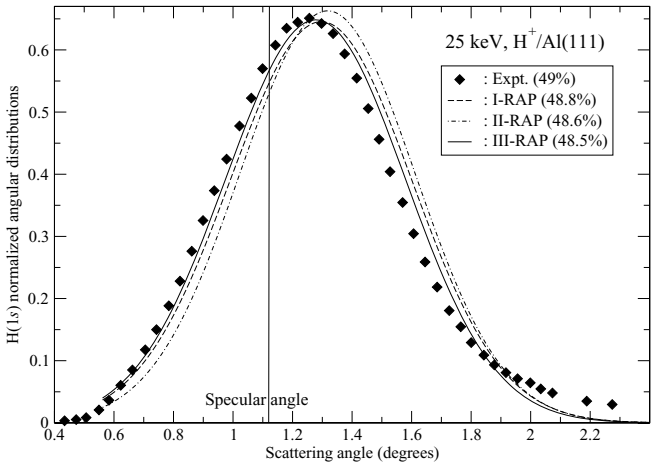

FIG. 3. Normalized ADs of scattered H(1*s*) atoms after grazing (0.56°) collisions of 25-keV H^+ ions with an Al(111) surface as functions of the scattering angle. (Solid diamonds) Normalized (see text) experimental data of Ref. [12]. The three lines correspond to calculations performed by consideration of all the mechanisms: In all cases static Auger transition rates of Ref. [8] are used as well as our results for PSP transition rates. Dashed line, Ref. [5] for static resonant transition rates and atomic energy (Calculation I-RAP); dot-dashed line, Ref. [6] for static resonant transition rates and atomic energy (Calculation II-RAP); solid line, Ref. [7] for static resonant transition rates and atomic energy (Calculation III-RAP).

for corrugation effects. More explicitly, the convolution of the primary AD (see the beginning of Sec. II) by a Gaussian shape which presents a strong decrease at the tails is not able to reproduce the rather low vanishing behavior of the experimental result at large angles. The atoms represented by the large angle tail of the distributions correspond to that small portion of the incident protons whose last electronic capture (which for few of them might be the first one) occurs very close to the surface, a region where the image force is strong due to the large increment of the slope of the image potential (see Fig. 1). These protons suffer a large increment of their perpendicular velocity previous to their neutralization being as a consequence dispersed toward larger angles than most of the other projectiles.

Besides the previously discussed small difference at large angles between the experimental and the theoretical curves, the AD for the case II-RAP appears to be a little bit shifted toward larger angles with respect to I-RAP and III-RAP and also with respect to the experimental curve, an effect which is clearer near the peak of the distributions where the height of the AD-II becomes also the tallest. Both effects are a direct consequence of two characteristics of the transition rates in case II which are not present in the corresponding curves of cases I and III. One of these characteristics is the absence of saturation of the resonant rates in case II near the surface [and more specifically of resonant loss rates; see Figs. 2(a)–2(c)], which is clearly present in the equivalent curves in case III and also in case I (to a smaller degree). As a consequence, neutralization in cases I and III takes place at larger distances than in case II. Furthermore, in this latter case resonant loss dominates in the close image plane region [see Fig. 2(b)]. These effects lead to a production of neutrals more important near the surface in case II than in cases I and III. In this region, the dynamical image potential has its largest effect sending neutrals away from the specular angle and shifting on the average the AD-II curves with respect to the other two ADs. The other characteristic of the rates in case II which is not present in cases I and III is related to the fact that the surface-plasmon capture rate in case II at large distances overcomes all the other rates included the loss rates. In fact, it is the only case in which a capture rate is above all the loss rates and occurs at intermediate and long ion-surface distances. As a consequence, the amount of neutralization in case II is increased pushing up the whole AD at angles beyond the specular one leading to an increment of the peak's height for the AD-II curve with respect to the two others. The effect of the collective mode of neutralization on AD-II will be further illustrated when analyzing Fig. 4. Both effects (absence of saturation and collective contribution) work simultaneously to produce as a result both the shift and the rising of the curve AD-II with respect to the two other ones.

In Figs. 4(a)–4(c) the contributions (capture and loss) coming from the resonant (R) mode alone (for the cases I, II, and III considered in Fig. 2) are compared with the simultaneous contributions (capture and loss) from the resonant plus the Auger mode (RA) and with both the total AD (capture and loss, RAP) and the experimental results already displayed in Fig. 3. Since from the results obtained from the transition rates (Fig. 2) and from the previous study of NFs in Ref. [2] it is clear that the most relevant mode of ion neutralization for the H^+-Al at 25 keV is the resonant mode,

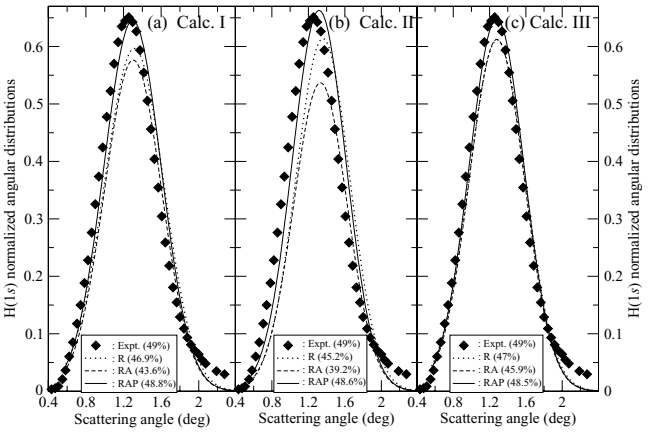

FIG. 4. Normalized ADs of scattered H(1s) atoms after grazing (0.56°) collisions of 25-keV H^+ ions with an Al(111) surface as functions of the scattering angle. (a) Calculation I, (b) calculation II, (c) calculation III (see text). (Solid diamonds) Normalized (see text) experimental result reported in Ref. [12]. Dotted lines, calculations R (contribution of resonant processes alone); dashed lines, calculations RA (contributions of resonant and Auger processes); solid lines, calculations RAP (all mechanisms are included).

it is not of much significance to include the equivalent results for the Auger mode alone. Similarly, for the collective mode (P) we do not consider it alone since neutralization is mostly dominated by the resonant (complemented by the Auger mode) and also because we have excluded the possibility of collective loss in such a way that evaluations of AD based only on the collective mode would be meaningless. We find that:

(1) The resonant mode represents the most important contribution to the total AD for the three cases under consideration.

(2) For all these cases the differences between the RA curves and the RAP curves are significative. Thus, since the RAP curves are in good agreement with the experimental result, we conclude that the plasmon contribution is important in order to reach the good agreement between theory and experiment independent of the approach followed for the resonant mode. In practice, the collective mode increases the calculated AD to reach the same height at its maximum as the experimental one keeping at the same time its width very close to the one of the experimental distribution.

(3) Note that in cases I and II, when the Auger mode is added to the resonant mode, the corresponding RA curves go below the equivalent R curves (with a smaller fraction of neutrals), while in case III the R curve is practically not affected by the contribution of the Auger mode. The explanation is related to the three following points:

(a) In case I the Auger capture rate goes clearly below the Auger loss one in the whole range of ion-surface distances while the capture and loss rates for the resonant mode go very close to each other and sufficiently above both Auger rates except very near the surface. Therefore, when the Auger mode is included together with the resonant mode, the action of the Auger loss channel (which is more efficient than the Auger capture channel) helps to introduce on the average an extra amount of ionization of the projectiles decreasing both the AD curve and as a consequence the final number of neutrals.

(b) In case II (as in case I), the rate for the Auger capture channel goes clearly below the rate for the Auger loss channel. However, as opposed to case I, the capture and loss resonant rates also go below the Auger loss rates for most of the range of ion-surface distances. Therefore, when the Auger mode is considered simultaneously with the resonant mode, the ionization of neutrals gets even more efficient than in case I. As a consequence, the final number of neutrals is even lower than in case I with the curve RA clearly below the curve R and with a significative smaller amount of NF.

(c) In case III the resonant rates go almost an order of magnitude above the Auger rates for most of the range of ion-surface distances except very close to the surface, where the Auger loss channel is comparable or slightly larger than both resonant channels, in such a way that the inclusion of the Auger mode will affect very weakly the results obtained with the resonant mode. Therefore, differences between curves R and RA are very small with a rather small decrease of the final NF.

We have also performed various other tests calculations in which different combinations of the charge transfer processes have been considered (RP, AP, . . .). The corresponding results are not reported here for the sake of conciseness. These test results confirm the fact that calculations in which all the charge-transfer processes are taken into account (RAP) are closer to the experimental data than those where one of the processes is not included, whatever the static resonant result considered.

As already mentioned in the Introduction, another important ingredient in the evaluation of the AD is the image potential interaction between the ions and the surface. In the preceding results we have considered the potential proposed by GAE [4], while in earlier works for helium ions interacting with Al surfaces at low energies we have applied the static (velocity independent) potential proposed by Kato *et al.* (K) [16] which was obtained within the Thomas-Fermi approximation. In order to analyze both the sensitivity of the theoretical AD to these potentials and their compatibility with the experimental data, we compare in Figs. 5(a)–5(c) their corresponding total (RAP) ADs for the three static resonant rates considered previously. For completeness and also as a reference, the experimental results [12] shown in Fig. 3 are also included in Figs. 5(a)–5(c). We have already concluded from Fig. 3 that the GAE potential yields a good overall agreement between the experimental curve and the three theoretical ADs related to the three static resonant cases under consideration. In the three cases, the use of the Kato *et al.* image potential lead to NFs which are very close to those obtained by means of the GAE one (the relevant NF values are reported on Fig. 5). Furthermore, in case II, both image potentials provide ADs which are almost identical in the whole range of angles. However, in cases I and III, ADs obtained by consideration of the Kato *et al.* potential are slightly broadened with respect to those obtained with the GAE potential. Consequently, the height of the corresponding peaks are significantly lower with the Kato *et al.* potential (since NFs are almost the same with both potentials) and the agreement with experiment is somewhat lost. This situation can be understood by noting that the neutralization zone is more localized in case II than in cases I and III due to the absence of a saturation region for the

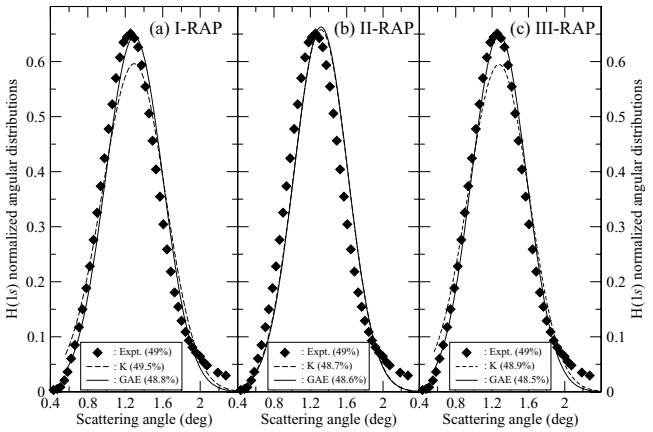

FIG. 5. Normalized ADs of scattered H(1s) atoms after grazing (0.56°) collisions of 25-keV H^+ ions with an Al(111) surface as functions of the scattering angle. (a) Calculation I-RAP, (b) calculation II-RAP, (c) calculation III-RAP (see text). (Solid diamonds) Normalized (see text) experimental data of Ref. [12]. Solid lines, results obtained by using the dynamical image potential of Garcia de Abajo and Echenique [4]; dashed lines, results obtained by means of the static image potential of Kato *et al.* [16].

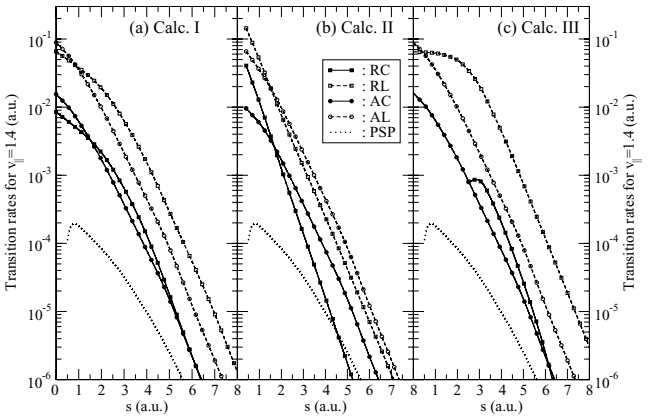

FIG. 6. $v_\parallel = 1.4$ a.u. (49-keV) transition rates for RC (solid squares), RL (open squares), AC (filled circles), AL (open circles), and PSP (dotted line) processes as a function of the particle-image plane distance (s). (a) Calculation I, based on static results of Refs. [5] and [8]; (b) Calculation II, based on static results of Refs. [6] and [8]; (c) Calculation III, based on static results of Refs. [7] and [8] (see text).

transition rates in case II (see Fig. 2). In that way, cases I and III are more sensitives to changes in the particle's velocities as those induced by the use of the Kato *et al.* potential instead of the GAE one (see Fig. 1).

As a partial conclusion of the present comparisons between calculations and the experimental AD at 25 keV, it seems that the static resonant results of Refs. [5] and [7] make it possible to better account for the experiment than those of Ref. [6] (see Fig. 3). Nevertheless, such a statement has to be confirmed by more extensive comparisons between theoretical and experimental ADs for other impact energies.

B. Other incident energies

For the system under consideration here, we have not found in the literature information of experimental ADs involving other velocities than the one considered in the earlier section of this work ($v = 1.0$ a.u.). However, in order to know the effects of the projectile velocity on the AD for the present system and also to get a more complete understanding of the whole process of neutralization, we include in what follows results and discussions of theoretical ADs for the H^+-Al(111) system for velocities $v \neq 1.0$.

1. ADs for different neutral fractions (49- and 6.25-keV cases)

From the calculations performed in [2] we knew that for $v = 1$ a.u. the NFs obtained with the three different reports for the static resonant mode [5–7] were the same. Therefore, it was not too surprising to find out that the corresponding ADs (cases I, II, and III) discussed in the previous section were very close to each other. Under this circumstance, one might wonder what would be the situation for those velocities whose NFs for the three cases are known to be different [2]: Are these differences shown (decreased or increased) by the corresponding ADs? To answer this question we have calculated the ADs (cases I, II, and III) for impact velocities $v = 1.4$ a.u. (49 keV) and $v = 0.5$ a.u. (6.25 keV) whose corresponding NFs (cases I, II, and III) were found in Ref. [2] to show noticeable differences.

In Fig. 6, resonant and Auger capture and loss transition rates are given for $v_\parallel = 1.4$ for the three different calculations (I–III) considered previously. As in Fig. 2, for purposes of completeness, we also include the rates of the corresponding surface-plasmon neutralization mode [2,10]. From Fig. 6, one can see that:

(i) For the three cases the rates for the loss channels clearly overcome those for the capture channel for both the resonant and the Auger modes, something to be expected since $v_\parallel(=1.4) > v_F(=0.9)$. As a consequence, for this velocity neutralization is greatly reduced with respect to the previous $v_\parallel = 1.0$ case. The physical reason is connected to the fact that for this high-impact velocity there are only few electrons in the metal with enough speed to "catch" the fast proton.

(ii) The PSP rates are negligible as compared to all the other rates. The only exception, related to the resonant capture rate in case II, occurs at ion-surface distances where the PSP value is orders of magnitude smaller than the values of the other rates. Therefore, one can expect that in this case the PSP contribution will be very weak.

(iii) In cases I and III for ion surfaces not too small ($s \gtrsim 1$) the resonant loss rate overcomes all other rates, while in case II it is the Auger loss rate that goes above the other rates. This pattern is qualitatively similar to the one for $v_\parallel = 1.0$, although now the corresponding capture rates go well below the loss rates.

The results of the calculations for the ADs are shown in Fig. 7. We see that for the three cases the high velocity of the incident protons (yielding capture rates well below the corresponding loss rates) largely reduce the final fractions of neutrals as compared to those for $v_\parallel = 1.0$. Another important distinctive feature of the ADs for $v_\parallel = 1.4$ is related to the large differences between the three AD curves which do not overlap. Furthermore, the heights of the three peaks are very

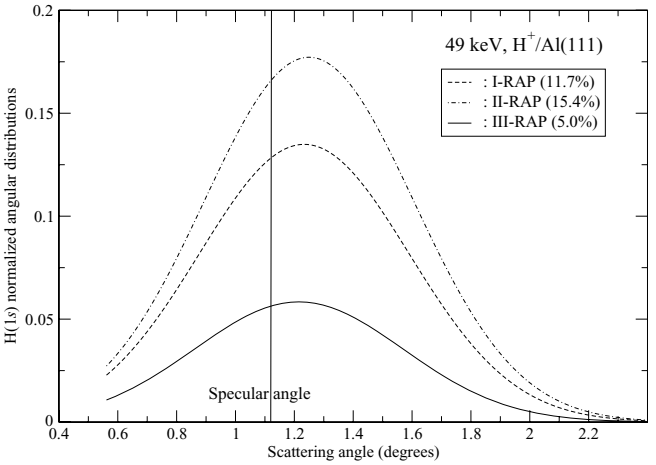

FIG. 7. Normalized ADs of scattered H(1s) atoms after grazing (0.56°) collisions of 49-keV H^+ ions with an Al(111) surface as functions of the scattering angle. The three lines correspond to calculations performed by consideration of all the mechanisms: In all cases static Auger transition rates of Ref. [8] are used, as well as our results for PSP transition rates. Dashed line, Ref. [5] for static resonant transition rates and atomic energy (Calculation I-RAP); dot-dashed line, Ref. [6] for static resonant transition rates and atomic energy (Calculation II-RAP); solid line, Ref. [7] for static resonant transition rates and atomic energy (Calculation III-RAP).

different and with almost negligible shifts with respect to each other. The smallest neutralization for case III is explained by the large values of both resonant and Auger loss rates above the corresponding capture rates as shown in Fig. 6(c). A similar explanation is valid for curve I, although for this case the capture channels are closer to the loss channels for both resonant and Auger modes increasing the amount of neutralization. Finally, the largest neutralization obtained in case II is related to the important values obtained for the resonant capture rate at short distances making it to compete strongly with both loss channels. It must be noted that the NF obtained in case I (11.7%) is closer to the experimental [1] result (9 ± 2%) than those obtained with the two other calculations.

Next, in Figs. 8 and 9 we show results for $v_\parallel = 0.5$ which are equivalents to those presented in the two preceding

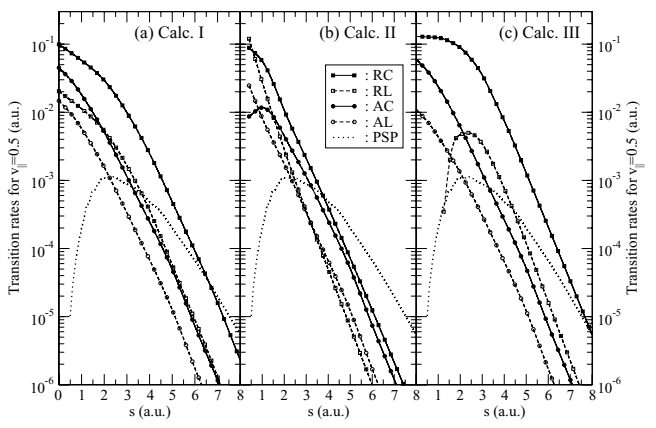

FIG. 8. Same as Fig. 6 for $v_\parallel = 0.5$ a.u. (6.25 keV).

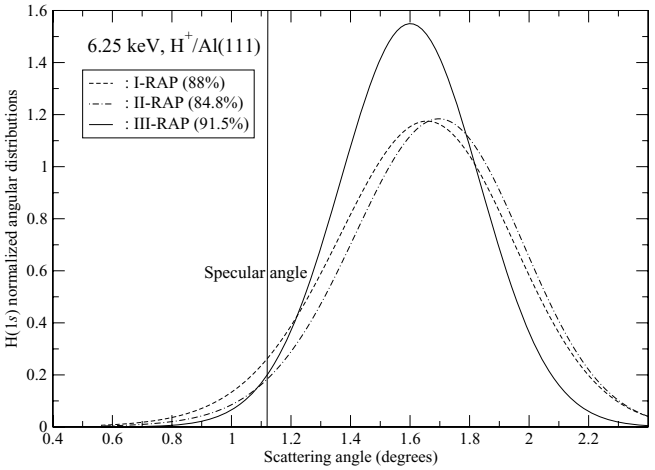

FIG. 9. Same as Fig. 7 for an incident energy of 6.25 keV.

figures (for transition rates and for ADs, respectively). One can see from Fig. 8 that for $v_\parallel = 0.5$ both the resonant and the Auger capture rates largely overcome the corresponding loss channels, contrary to what happens in the high-velocity regime ($v_\parallel > v_F$). This situation is evident at all ion-surface distances for cases I and III, while in case II the same is true for ion distances not too close to the surface. Furthermore, the plasmon rates become significatively more important (with respect to both the resonant and the Auger modes) for $v_\parallel = 0.5$ than for the high-velocity regime, especially for case II at intermediate and large ion-surface distances, where it becomes the largest rate. At this velocity, neutralization is more important than for $v_\parallel = 1.4$ and $v_\parallel = 1.0$ in accord with the NFs obtained in Ref. [2]. One interesting feature of these rates, which was absent in all the capture and loss rates for both the resonant and the Auger modes considered so far in this work, is the appearance in case II of a maximum for the Auger capture rate. The corresponding Auger loss rate does not show this behavior. It means that the highest probability contribution of this capture rate to the total neutralization will be at distances away from the surface contrary to the other cases where the probability contribution increases until the surface is reached.

Figure 9 shows the ADs for the three cases. The pattern of the three curves is clearly different than the one found for $v_\parallel = 1.0$ and for $v_\parallel = 1.4$. First at all, the angular shift between these curves was not present for $v_\parallel = 1.4$, while for $v_\parallel = 1.0$ it was relatively small. Second, the height of each peak is much larger than the corresponding value for the higher velocities, while the relative differences between the peaks are smaller than for $v_\parallel = 1.4$ but larger than for $v_\parallel = 1.0$. Therefore, again, different NFs are related to different ADs. However, one sees that the differences made explicit by the ADs for the three cases are much more informative than those from the NFs. Indeed, we see from Fig. 9 that the AD for case III is narrower than the other two curves (which do not differ too much from each other), with its larger peak shifted toward smaller angles. Therefore, both the trajectories followed by the projectiles and their final directions obtained from calculation III are noticeably different than those represented by calculations I and II. Furthermore, one has to note that the NF obtained from

case III (91.5%) is closer to the experimental value (97%) than those obtained from cases I and II. The explanation of the AD curves for $v_\parallel = 0.5$ in terms of the corresponding rates given in Fig. 8 follow the same lines as those for $v_\parallel = 1.0$ and $v_\parallel = 1.4$, so we do not include them here.

From the preceding results it is clear that different NFs are related to noticeably different ADs independent of the velocity of the incoming ions, something which is to be expected if one has in mind the connection between these two physical quantities. For the last two situations ($v_\parallel = 1.4$ and $v_\parallel = 0.5$), the corresponding experimental data for the ADs (not found so far in the literature) would help to decide which of the curves (if any) represents better the correct description of these phenomena. In particular, the correct description of the static resonant mode might be connected with that theoretical AD curve which agrees reasonably well with the experimental data if the assumption that the rates of the Auger and surface-plasmon modes together with the description of the ion-surface interaction potential is correct.

2. *ADs for complete neutralization (1-keV case)*

From [2] it was also concluded that for projectile velocities less than 0.3 a.u. (and for the angle of incidence considered here) the three different static resonant rates lead to the complete neutralization of the proton beam, in agreement with the experimental data [1]. From this result, and having also in mind the conclusions we obtained for $v = 1.0$, one might be tempted to infer that for any projectile velocity in the range $0 \lesssim v \lesssim 0.3$ the corresponding ADs (cases I, II, and III) will be very close to each other. To study this situation in some detail, we have performed calculations of AD for the impact velocity $v = 0.2$. In Fig. 10 we report the relevant transition rates as functions of the ion-surface distances, while in Fig. 11 we show the corresponding ADs.

A simple look at the transition rates reported in Fig. 10 indicates that:

(a) The capture rates for both the resonant and the Auger modes are overwhelmingly stronger than the corresponding loss rates in the whole range of relevant distances. In cases I and III, the resonant loss rates are zero while in case II it is finite only in a very small window of distances very close to the surface where it gets close and even surpasses the resonant capture mode. These features are related to the different forms

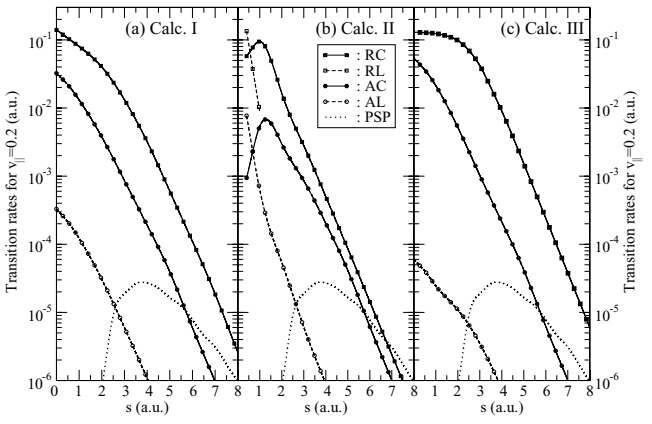

FIG. 10. Same as Fig. 8 for $v_\parallel = 0.2$ a.u. (1 keV).

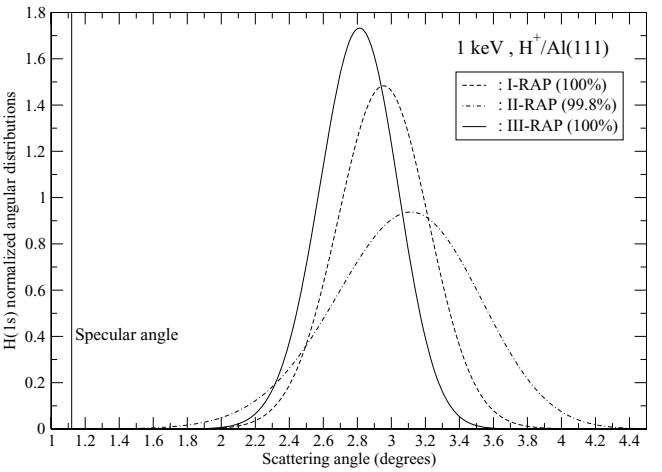

FIG. 11. Same as Fig. 9 for an incident energy of 1 keV (note that the scaling of the horizontal axis is different from the one used in the equivalent Figs. 3, 7, and 9).

of the H(1s) energy shift reported in [5–7]. Similarly, even though the Auger loss rates are finite, they are several orders of magnitude smaller than the Auger capture rates. This situation represents a strong reinforcement of the tendency of theses rates already observed in going from $v_\parallel = 1.0$ to $v_\parallel = 0.5$. Therefore, it does not come as a surprise to expect NFs for $v = 0.2$ well above those obtained for $v = 0.5$.

(b) On the contrary, the surface-plasmon rates appear strongly disminished as compared to the resonant and Auger capture rates due to both the increment of the latter rates and a lowering of the collective rate at this velocity, as analyzed in Refs. [2,10]. Therefore, at $v_\parallel = 0.2$ the contribution of the collective mode is expected to be pretty weak, being closer to what happens for $v_\parallel = 1.4$ than to those contributions reported for the velocities $v_\parallel = 1.0$ and $v_\parallel = 0.5$.

(c) An extra feature of our results at $v_\parallel = 0.2$ is the presence, in case II, of a maximum in both the resonant and the Auger capture rates, a situation which we first found also for case II at $v_\parallel = 0.5$ but only for the Auger capture mode. As a consequence in this case, both capture rates contribute to pushing away from the surface the neutralization as opposed to cases I and III.

For the corresponding ADs, from Fig. 11 we see that:

(1) The ADs for the three cases (I, II, and III) are clearly higher at their maximum and also wider than the corresponding curves for $v = 0.5$. The AD for case III is both the tallest and the narrowest of the three distributions, while curve II has the lowest height, being the widest of the three curves. Finally, the height for the distribution of case II is approximately half way between the heights of the other two curves and the same as its width.

(2) The consequences of the preceding behavior is that the three curves get (approximately) full neutralization. Probably the fact that in case II 100% of the neutralization is not reached is related to the fact that for the resonant and the Auger modes the loss rates surpass the corresponding capture rates in a small region close to the surface.

However, the most important conclusion of this calculations is that equal NFs can be obtained for totally different ADs. In this sense for the range of impact velocities $v \lesssim 0.3$

the NFs are completely blind to the characteristic of the neutralization process. However, the ADs can discriminate clearly the different trajectories of the projectiles, how they get distributed in angle, and how they get affected by the values of the rates which are relevant to the neutralization process.

IV. CONCLUSIONS

In the present work we have evaluated ADs for four representative velocities of H^+ projectiles ($v = 1.4$, 1.0, 0.5, and 0.2 a.u.) impinging upon an Al(111) surface under an angle of incidence of 0.56°. Since experimental results for these ADs have been reported in the literature only for $v = 1.0$ a.u., the other results for ADs reported here represent predictions which must be verified experimentally. An important feature of these calculations is that for each of the aforementioned velocities we have used three different reports for the static resonant rates (eigenenergies and widths) [5–7] in order to evaluate first velocity-dependent resonant and Auger (capture and loss) rates which afterward are included, together with collective rates for ion neutralization plus the ion-surface potential, in the numerical ETISC1D code [3] for dynamical calculations. As a consequence of such calculations, ADs and NFs are simultaneously obtained for each velocity and for each static resonant case under consideration. For thoses cases where there is no experimental information a comparison between the predicted AD and new experimental data might give some light into which (if any) of the static resonance rates proposed in the literature and considered in this work [5–7] better account for the measurements.

Besides the results and conclusions analyzed in the previous sections, we want to mention in what follows a few other general tendencies shown by both the transition rates and the different sets of ADs, for the three cases under consideration, as functions of the projectile velocity:

(1) We already mentioned that for both resonant and Auger rates the ratio ($\mathcal{R}$) between the loss and the capture channels is larger than 1 for $v_\parallel > v_F$, equal to 1 for $v_\parallel = v_F$, and smaller than 1 for $v_\parallel < v_F$. More specifically, it is seen that for $v_\parallel \gg v_F$ one finds that $\mathcal{R} \gg 1$, while for $v_\parallel \ll v_F$ one gets $\mathcal{R} \ll 1$. On the other hand, the collective capture rate gets its highest value around v_F, decreasing quickly as the ion velocity gets too small or too large. A detailed discussion about the behavior of velocity dependent collective rates for the system under consideration is given in Ref. [2].

(2) An important consequence of the preceding behavior of the transition rates is that as the ion velocity goes down the NFs get largely increased until they reach their highest value of approximately 100% in the range $v \lesssim 0.3$. Another important consequence is that as the velocity decreases there is a clear increment of the shift of the AD's peak with respect to the specular angle. The explanation is related to the fact that at low velocities $\mathcal{R} \ll 1$, with the probability becoming largest at short distances of the surface where the image potential gets stronger, so that most of the particles suffer an important increment of their perpendicular velocity being sent to larger angles producing the shift of the whole AD at large angles as the impact velocity decreases.

(3) At the highest velocity considered in this work ($v = 1.4$), the AD curve for case III is the lowest one. However, as the ion velocity decreases it rises until it becomes the one with the largest peak in the whole intermediate and low-velocity range. For case II the situation is exactly the opposite, reaching the highest peak at high velocities but the smallest one at low velocities. Finally, for case I the velocity clearly affect the height of its peak but in such a way that it always remains between the other two cases, especially at the extremes of the velocity range under consideration, being very close to curve II in the intermediate range of velocities. The fact that for $v \lesssim 0.3$ the curves I, II, and III get the same amount of neutralization even though the height of the peaks of their ADs are very different indicates, in agreement with Fig. 11, that their widths are very different in order to reproduce an equal area under each curve (representing each NF) for the three cases studied in this work.

Finally, we mention that ADs for neutral hydrogen atoms H^0 impinging on Al surfaces are also given in Ref. [12] under the same geometrical and energy conditions as the system analyzed in this work. Work is in progress to study the behavior of the ADs for this system and to obtain the values of the corresponding NFs as functions of the velocity of the projectile.

ACKNOWLEDGMENTS

The collaboration between the "Sources X, Plasmas and Ions" Group at CELIA (Bordeaux, France) and the Atomic Collision Group at the Universidad de Concepción, Chile, has been partially supported by the projects FONDECYT (regular) 1061003 and FONDECYT (Colaboracion Internacional) 7080171 and 7090091.

[1] H. Winter, Phys. Rep. **367**, 387 (2002).
[2] H. Jouin and F. A. Gutierrez, Phys. Rev. A **80**, 042901 (2009).
[3] S. Jequier, H. Jouin, C. Harel, and F. A. Gutierrez, Surf. Sci. **570**, 189 (2004).
[4] F. J. Garcia de Abajo and P. M. Echenique, Phys. Rev. B **48**, 13399 (1993).
[5] P. Nordlander and J. C. Tully, Phys. Rev. B **42**, 5564 (1990).
[6] A. G. Borisov, D. Teillet-Billy, and J. P. Gauyacq, Nucl. Instrum. Methods Phys. Res. B **78**, 49 (1993).
[7] S. A. Deutscher, X. Yang, and J. Burgdörfer, Phys. Rev. A **55**, 466 (1997).
[8] R. Hentschke, K. J. Snowdon, P. Hertel, and W. Heiland, Surf. Sci. **173**, 565 (1986).
[9] Z. L. Mišković and R. K. Janev, Surf. Sci. **221**, 317 (1989).
[10] R. Sandoval, F. A. Gutierrez, and H. Jouin, Nucl. Instrum. Methods Phys. Res. B **258**, 44 (2007).
[11] R. Zimny, Z. L. Mišković, N. N. Nedeljković, and Lj. D. Nedeljković, Surf. Sci. **255**, 135 (1991).
[12] H. Winter and M. Sommer, Phys. Lett. A **168**, 409 (1992).
[13] T. Hecht, H. Winter, and A. G. Borisov, Surf. Sci. **406**, L607 (1998).
[14] J. P. Ziegler, J. P. Biersack, and U. Littmark, *The Stopping and Range of Ions in Solids* (Pergamon, New York, 1985).

[15] P. A. Serena, J. M. Soler, and N. Garcia, Europhys. Lett. **8**, 185 (1989).
[16] M. Kato, R. S. Williams, and M. Aono, Nucl. Instrum. Methods Phys. Res. B **33**, 462 (1988).
[17] H. Jouin, F. A. Gutierrez, and C. Harel, Phys. Rev. A **63**, 052901 (2001).
[18] F. A. Gutierrez, H. Jouin, J. Díaz-Valdés, and A. R. Matamala, Physica A **359**, 430 (2006).
[19] F. Martín and M. E. Politis, Surf. Sci. **356**, 247 (1996).
[20] P. Kurpick, U. Thumm, and U. Wille, Phys. Rev. A **56**, 543 (1997).
[21] P. J. Jennings, R. O. Jones, and M. Weinert, Phys. Rev. B **37**, 6113 (1988).
[22] F. A. Gutierrez and H. Jouin, Phys. Rev. A **68**, 012903 (2003).